frontiers | Frontiers in Earth Science

TYPE Original Research
PUBLISHED 17 January 2023
DOI 10.3389/feart.2022.1041374

OPEN ACCESS

EDITED BY
Harry F. Lee,
The Chinese University of Hong Kong, China

REVIEWED BY
Fang Tian,
Capital Normal University, China
Xin Zhou,
University of Science and Technology of China, China

*CORRESPONDENCE
Yunfa Miao,
yunfine2000@sina.com
Zhiyong Ling,
lingzhiyong@foxmail.com

SPECIALTY SECTION
This article was submitted to Quaternary Science, Geomorphology and Paleoenvironment, a section of the journal Frontiers in Earth Science

RECEIVED 10 September 2022
ACCEPTED 27 October 2022
PUBLISHED 17 January 2023

CITATION
Liu P, Zhang S, Qiu M, Ruan Q, Luo J, Miao Y and Ling Z (2023), Vegetation history and its links to climate change during the last 36 ka in arid Central Asia: Evidence from a loess-paleosol sequence in the Eastern Ili Valley. *Front. Earth Sci.* 10:1041374. doi: 10.3389/feart.2022.1041374

Vegetation history and its links to climate change during the last 36 ka in arid Central Asia: Evidence from a loess-paleosol sequence in the Eastern Ili Valley

Peilun Liu[1,2,3], Shanjia Zhang[1], Menghan Qiu[1], Qiurong Ruan[4], Jiaming Luo[4], Yunfa Miao[2]* and Zhiyong Ling[5]*

[1]Key Laboratory of Western China's Environmental Systems, Lanzhou University, Lanzhou, China, [2]Key Laboratory of Desert and Desertification, Northwest Institute of Eco-Environment and Resources, Chinese Academy of Sciences, Lanzhou, China, [3]College of Resources and Environment, University of Chinese Academy of Sciences, Beijing, China, [4]Institute of Cultural Relics and Archaeology in Xinjiang, Urumqi, China, [5]Key Laboratory of Comprehensive and Highly Efficient Utilization of Salt Lake Resources, Qinghai Provincial Key Laboratory of Geology and Environment of Salt Lakes, Qinghai Institute of Salt Lakes, Xining, China

Detailed vegetation history response to complex influencing factors of arid Central Asia (ACA) is crucial to understanding ecological sustainability. Here, we present the first pollen record in the Ili Valley during the Last Glacial Maximum (LGM) using the Jirentai (JRT) loess-paleosol sequence. Combining the results of multi-climate proxies and optically stimulated luminescence (OSL) dating, we aim to reconstruct the vegetative response to climate change during the last 36 ka. Our results show that rapid loess accumulation in the JRT section began in the Late MIS3 (Marine isotope stage 3), and a thin paleosol layer developed in the Late LGM and Post Glacial. The pollen concentrations in the loess are significantly lower than in the paleosol, but the pollen assemblages are richer. *Artemisia* and *Asteraceae* are the dominant non-arboreal types in the loess, and abundant arboreal species are present (e.g., *Pinus*, *Picea, Quercus,* Betulaceae). The percentage of *Artemisia* remains high in the paleosol, and typical drought-tolerant plants are an important component (e.g., Orthomorphic, *Ephedra*). We suggest that the rich variety of pollen in loess is transported by frequent and intense dust activities, and these pollen may come from regional vegetation. Less diverse pollen assemblages in paleosol respond to the vegetation surrounding the JRT section. The vegetation history obtained from the JRT section shows that the lowlands of the Ili Valley were typical desert or desert-steppe vegetation for the past 36 ka. The surrounding mountains are dominated by *Pinus* and *Picea* forests. During the Early LGM, vegetation conditions deteriorated in both of mountainous and lowland. The above phenomena coincide with the pollen records from lakes in the ACA. Our results further suggest that mountain forests reappear and the lowland environment improves in response to increased insolation in the Northern Hemisphere at high latitudes in the Late LGM. This point in time is earlier by about 5–10 ka compared to previous records. We attribute it to the fact that pollen assemblages from the loess-paleosol sequence are more sensitive to vegetation and climate change

during the transition from the glacial to interglacial and propose a simple model to characterize them.

KEYWORDS

vegetation, Central Asia, ili valley, last glacial maximum, loess-paleosol sequence, pollen

1 Introduction

Vegetation history and its response to complex influencing factors (e.g., climate change, human activities) are beneficial to addressing the frequent extreme events that are expected in a future global warming scenario (Li et al., 2018; Lu et al., 2019; Fordham et al., 2020; Mottl et al., 2021; Zhang et al., 2022). The ACA is one of the driest regions in the world. The mean annual precipitation (MAP) in most areas is less than 300 mm, while evaporation is several times higher than precipitation. Thus, this region is dominated by temperate desert, Gobi, and sandy land (Narisma et al., 2007; Chen et al., 2008). At the same time, the ACA is known as an important source of global dust activities (Prospero et al., 2002; Uno et al., 2009; Marx et al., 2018). In addition, the ecology of the ACA has become increasingly fragile over the past half-century. Increased water scarcity and significant expansion of desert areas are prominent due to global warming and population growth (Chen et al., 2011; Siegfried et al., 2012; Hu and Han., 2022). Therefore, it is crucial to proceed with the reconstruction of vegetation history at different spatial and temporal scales in the ACA.

Abundant Late Quaternary paleoclimatic researches have been carried out in the ACA to investigate the relationships between climate change and environmental conditions, as well as to predict and respond to possible ecological crises (Yao et al., 1997; Chen et al., 2008; Wang and Feng, 2013). In the present Holocene Interglacial, the precipitation pattern of the ACA is dominated by the westerlies. In contrast to the East Asian monsoon region, relatively wet conditions occurred in the middle to late Holocene (Chen et al., 2016; Chen et al., 2019). At the glacial-interglacial scale, climate change in the ACA is synchronized with the East Asian monsoon region. Both regions are controlled by global ice volume and display a cold-dry climatic pattern in the glacial period (Ding et al., 2002; Li et al., 2016; Yang et al., 2020).

Pollen is an excellent indicator of vegetation history (Miao et al., 2017; Chevaliera et al., 2020; Zhao et al., 2021; Li et al., 2022). At present, only a small number of pollen records have been used to reconstruct the vegetation history in the ACA during the Last Glacial, such as lakes Manas, Balikun, Ebi, and Ailike (Rhodes et al., 1996; Tao et al., 2010; An et al., 2013; Zhao et al., 2015; Jia et al., 2020; Chen and Liu., 2022). These records reflect the severe deterioration of vegetation condition in the ACA during the LGM. However, due to lower sedimentation rates, low-resolution sediments from glacial periods provide noticeably less information than during the interglacial. Since the Late Quaternary, aeolian deposits have been widely distributed in the ACA and thicker sediments formed under cold and windy conditions (Li et al., 2016; Song et al., 2021; Li et al., 2022). They provide ideal materials for targeted reconstruction of the vegetation history within the glacial.

The Ili Valley is situated in the northeastern part of the ACA (Figure 1). Within the Holocene stage, it belongs to the core area of the "westerlies-dominated climate regime" (Chen et al., 2019). The prevailing westerly winds bring abundant precipitation to the river valley and surrounding mountains (Ye et al., 2000). A lacustrine section from the Ili Valley had been used to reconstruct the vegetation history since the Late MIS3. However, it is lacking the sediment during the LGM (Li et al., 2011; Zhao et al., 2013; Zhao et al., 2019). The dust dynamics of aeolian deposits in the Ili Valley have been well studied during the Last Glacial, and the accumulation rate is mainly influenced by the Siberian High-pressure system (Li et al., 2019; Yang et al., 2020; Kang et al., 2022). Here, using a loess-paleosol sequence collected near the Jirentai site on the second terrace of the Kashi River as material, we provide the first pollen record from the Ili Valley during the LGM with luminescence dating and the results of multi-climate proxies (e.g., grain size, magnetic susceptibility, total organic carbon (TOC), and elemental content). Furthermore, we reconstructed the vegetation history for the past ~36 ka and explored its links to climate change. Finally, we compared the changing characteristics of pollen records from lake sediments and the loess-paleosol sequence in the ACA during this period and point out the advantages of using aeolian deposits to reconstruct arid zone vegetation in the glacial period.

2 Study area

The Ili Valley is located in Central Asia and is surrounded by the Tian Shan orogenic belt. The topography of the valley has a trumpet shape that narrows from west to east and gradually increases in elevation. Despite being part of the same westerlies-dominated climatic regime as the vast adjacent desert, such as the Saryesik-Atyrau Desert and the Taklamakan Desert (Figure 1). The special topography hinders the mid-latitude westerlies and brings more abundant precipitation to the Ili Valley, especially in the late spring and summer (Shi et al., 2007). The MAP of the region is between 200 and 500 mm, with accumulations of up to 1000 mm in the high mountains. The

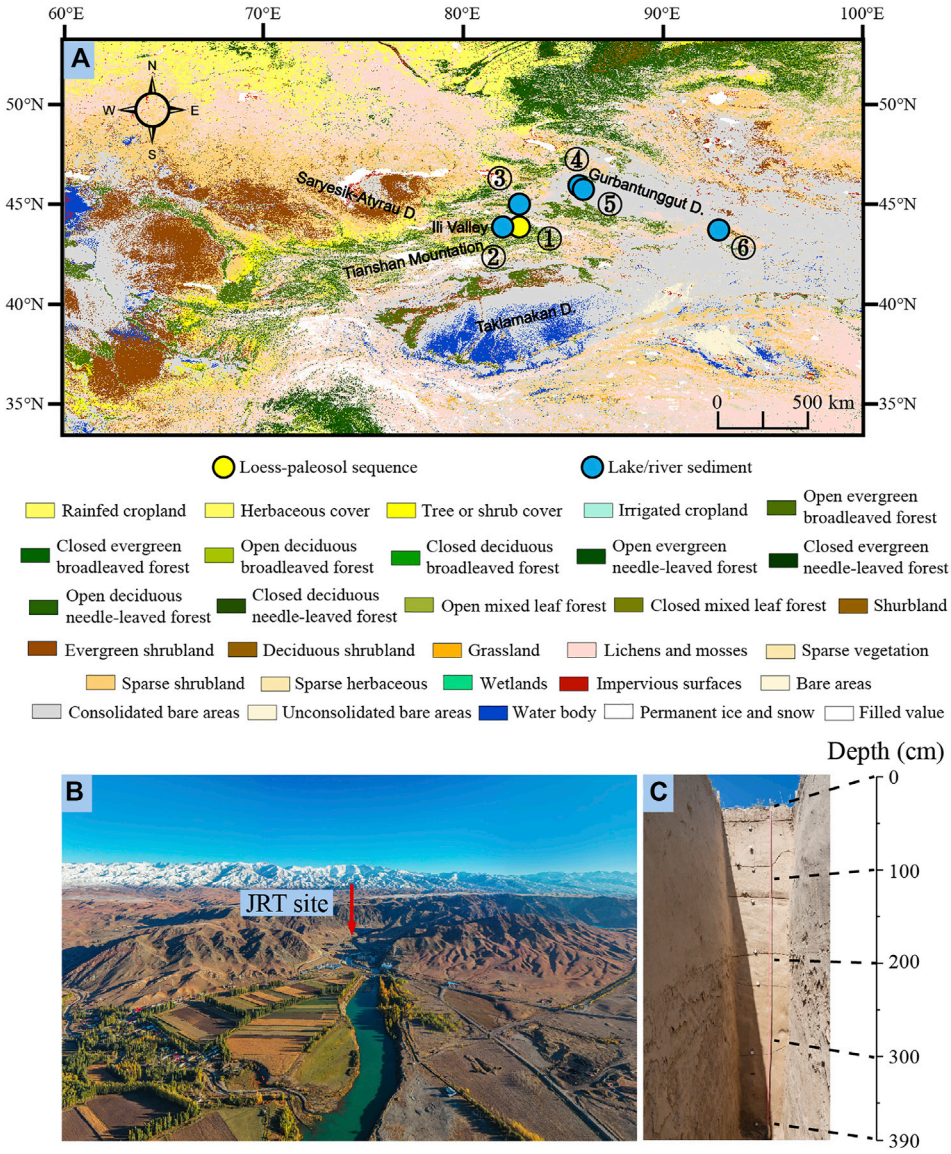

FIGURE 1
Land cover and geomorphology around the Ili Valley in ACA (The land cover data in panel **(A)** are derived from Liu and Zhang (2021)). **(A)** Location of the JRT section and other pollen records mentioned in this paper (1. JRT section, this study; 2. Yili section (Li et al., 2011); 3. Lake Abi; 4. Lake Ailike; 5. Lake Manas; 6. Lake Bilikun); **(B)** Environmental conditions surrounding the JRT section; **(C)** JRT section and OSL sampling depths.

rainfall in the mountains forms runoff that further shapes the environment of the lowlands, such as the Kashi River and Turks River (Xia et al., 2018). The mean annual temperature (MAT) ranges from 3 to 10°C. The natural environment of the Ili Valley is sensitive to climate change. Over the past half-century, the Ili Valley has been characterized by warming and humidification. The frequency of both extreme climate hazards and secondary hazards has also increased significantly (Li, 1991; Li et al., 2012; Wu et al., 2018).

The modern vegetation distribution has been used as a basis for reconstructing past vegetation-climate relationships. Greater evaporation at the bottom of Ili valley leads to drought in the lowlands. Consequently, the vegetation types below 1500 m above sea level (a.s.l.) are mainly montane steppe and desert (The main plant type are Poaceae, *Artemisia*, Asteraceae, Amaranthaceae). With the increasing altitude, the vegetation zones show a significant vertical zonality. Montane forest-meadow (e.g., Betulaceae, Lamiaceae, Poaceae, Rosaceae), subalpine meadow (e.g., Rosaceae, Geraniaceae, *Artemisia*), alpine meadow (e.g., *Artemisia*, Polygonaceae), and alpine cushion-like vegetation (e.g., Rosaceae, Caryophyllaceae) occur sequentially. Alpine coniferous forest zones (The main

establishment species is *Picea*) develop at altitudes up to 2800 m a.s.l. and represent the best vegetation condition (Xinjiang Expedition Team Chinese Academy of Sciences, 1978; Xu et al., 2010; Tian et al., 2012; Zhao and Li., 2013; Niu et al., 2022).

Aeolian deposits with significant differences in thickness are widely distributed on the piedmont and river terraces in the Ili Valley. Frequent dust activities in winter and spring triggered by Siberian High-pressure leads to an eastward transport of unsorted sediments on piedmont slopes and alluvial-riverine plains. Dune sediments from distant sources are also one of the material sources of aeolian deposition (Orlovsky et al., 2005; Youn et al., 2014; Li et al., 2020). Sediment thickness becomes thicker and then thinner with increasing elevation (Ye, 2001; Fang et al., 2002). Despite the differences in deposition rates due to topographic features, the aeolian accumulation rate in the Ili Valley is relatively high during the glacial period. These deposits thus provide an ideal terrestrial archive for reconstructing the vegetation history and climatic changes during this period (Youn et al., 2014; Li et al., 2016; Li et al., 2019).

3 Materials and methods

3.1 Jirentai section and field work

The Jirentai (JRT) section (82.78°E, 43.85°N, 1226 m a.s.l.) is located in eastern Ili Valley and overlays on the third terrace of the north bank of the Kashi River (Figure 1). The loess at this terrace has formed around 60 ka, and is piled on top of gravels (Zhang et al., 2021). It consists of undisturbed 3.9 m long wind-formed deposits with sparse weed growth on the surface. Based on field observations, a remarkable paleosol layer about 25 cm thick develops on a deep loess layer. We collected five samples at ~5 cm intervals at the top of the profile. In addition, 120 samples were collected at 1 cm intervals between 25 and 150 cm and 125 samples at 2 cm intervals between 150 and 390 cm. All 250 samples were measured for grain size, magnetic susceptibility, total organic carbon (TOC), and elemental content. In addition, to establish the age of the section, ten optically stimulated luminescence (OSL) dating samples were obtained from the sections at depths of 30, 60, 80, 90, 110, 130, 190, 230, 320, and 390 cm, respectively.

3.2 Climate proxy analyses

All soil samples were dry in their natural state. We weighed appropriate mass of samples for each of the four process-independent experiments. Extracting branches and leaves from the soil before performing the necessary pre-treatment process. The grain size was measured using a laser particle size analyzer, with a measurement range of 0.02–2000 μm and a systematic error of less than 2%. A Magix PW2403 X-ray fluorescence Xinjiang Expedition Team Chinese Academy of Sciences, 1978 analyzer was used to determine the elemental content of sediments with an analytical precision of better than 1–2%. The magnetic susceptibility was measured using a Bartington MS2B magnetic susceptibility meter at both low frequency (470 Hz) (χ_{lf}) and high frequency (4700 Hz) (χ_{hf}), and the mass-specific frequency-dependent magnetic susceptibility (χ_{fd}) was calculated by: $\chi_{fd} = \chi_{lf} - \chi_{hf}$, following. The TOC was measured using an elemental analyzer (Jena HT 1300 total carbon analyzer, Germany).

All experiments were conducted at the MOE Key Laboratory of Western China's Environmental System, Lanzhou University.

3.3 Optically stimulated luminescence dating sample measurement

Ten samples were used to extract minerals for equivalent dose (De) determination in a darkroom with a red light. After eliminating carbonates and organic matter, medium-grained (38–63 μm) quartz particles were extracted from samples and were selected as the material to construct a single-piece regeneration dose-standard curve (SAR-SGC) for dating (Murray and Wintle, 2000). Quartz grains were treated with 40% HF solution for 2 h to remove feldspar grains. Afterward, fluoride was removed from the obtained quartz particles with 10% HCl. The key to this process is to ensure that feldspar contamination is effectively removed to avoid underestimation of age. Luminescence measurements were collected using an automated Risø TL/OSL-DA-20 reader equipped with blue diodes (470 ± 20 nm) and IR laser diodes (830 nm). Irradiation was conducted using a 90Sr/90Y beta source built into the Risø reader. For the quartz samples used in this experiment, the natural and regenerative dose samples were treated with blue-emitting diodes. The Preheat temperatures was kept at 260°C for 10 s and the cut heat was 220°C for 10 s. The luminescence stimulation used blue LEDs at 130°C for 40 s, and the OSL signal was detected by a 9235QA photomultiplier tube through a 7.5-mm-thick Hoya U-340 filters. Signals over the first 1.6 s of stimulation were integrated for growth curve construction after background subtraction (final 8 s) to estimate the equivalent dose De value. The concentrations of U, Th, and K were determined using neutron activation analysis. Finally, the standard growth curve of Lx/Tx-Rx was established, and the natural light release signal intensity value LN/TN was inserted into the standard growth curve to find the equivalent dose value De (Murray and Wintle, 2000; Lai and Ou, 2003).

This experiment was conducted in the Light Release Laboratory, Qinghai Institute of Salt Lake, Chinese Academy of Sciences.

TABLE 1 OSL dating results of samples from the JRT section.

Sample Id	K (%)	Th (ppm)	U (ppm)	Water content (%)	Depth(m)	Dose rate (Gy/Ka)	De (Gy)	OSL age (ka)
JRTGKP-1	1.96 ± 0.04	12.56 ± 0.70	2.55 ± 0.40	6 ± 5	0.3	3.77 ± 0.28	23.8 ± 2.2	6.3 ± 0.7
JRTGKP-2	1.97 ± 0.04	12.05 ± 0.70	2.70 ± 0.40	6 ± 5	0.6	3.76 ± 0.28	84.9 ± 2.3	22.6 ± 1.8
JRTGKP-3	1.79 ± 0.04	10.89 ± 0.70	2.45 ± 0.30	6 ± 5	0.8	3.42 ± 0.25	73.7 ± 2.4	21.5 ± 1.7
JRTGKP-4	1.79 ± 0.04	12.13 ± 0.70	2.59 ± 0.40	6 ± 5	0.9	3.56 ± 0.27	79.1 ± 5.5	22.2 ± 2.3
JRTGKP-5	1.97 ± 0.04	11.71 ± 0.70	2.91 ± 0.40	6 ± 5	1.1	3.77 ± 0.28	89.8 ± 3.3	23.8 ± 2.0
JRTGKP-6	2.02 ± 0.04	11.93 ± 0.70	3.10 ± 0.40	6 ± 5	1.3	3.89 ± 0.29	90.9 ± 5.8	23.4 ± 2.3
JRTGKP-7	2.04 ± 0.04	12.81 ± 0.70	3.42 ± 0.40	8 ± 5	1.9	3.94 ± 0.29	117.7 ± 6.6	29.8 ± 2.8
JRTGKP-8	2.12 ± 0.04	12.52 ± 0.70	3.13 ± 0.40	8 ± 5	2.3	3.90 ± 0.29	117.3 ± 4.4	30.1 ± 2.5
JRTGKP-9	2.00 ± 0.04	12.60 ± 0.70	3.03 ± 0.40	8 ± 5	3.2	3.75 ± 0.28	125.7 ± 3.8	33.5 ± 2.7
JRTGKP-10	2.09 ± 0.04	13.92 ± 0.80	3.31 ± 0.40	8 ± 5	3.9	3.99 ± 0.30	125.9 ± 6.3	31.5 ± 2.8

3.4 Pollen analysis

In total, 46 samples were selected from the section for pollen analysis. After weighing 20 g of soil per sample for pre-treatment. A known number of *Lycopodium* spores (27637/slice) was added prior to the chemical treatment to calculate pollen concentrations. Solutions of 10% HCl and 10% HF were used to remove impurities, such as carbonate, nitrate and organic fractions. An ultrasonic shaker and a sieve cloth were used to further remove impurities smaller than 10 μm. The remaining material was preserved and made into samples. At least 300 grains of terrestrial plant pollen from each sample were identified under a microscope, or the entire sample was counted when the pollen count was insufficient. Pollen identification followed pollen atlases specific to the arid and semi-arid areas of China (Wang et al., 1995; Tang et al., 2016). Pollen diagrams were generated using Tilia v2.6.1 (Grimm, 1987; 2004).

This experiment was conducted in the Key Laboratory of Desert and Desertification, Northwest Institute of Eco-environment and Resources, Chinese Academy of Sciences.

4 Results

4.1 Optically stimulated luminescence dating results

The quartz OSL ages range from 6.3 ± 0.7 to 33.5 ± 2.7 ka. All the OSL ages are in stratigraphic order (within acceptable error) in the JRT section (Table 1). Based on direct dating results showing the top 30 cm of sediments formed in the middle to late Holocene, and aeolian sediments accumulated at depths between 130 and 60 cm in the LGM and 390–190 cm in the Late MIS3. The dating results are densely distributed in the LGM and Late MIS3, reflecting the rapid dust accumulation during this phase and also explaining part of the age reversal (e.g., JRTGKP-3)

Due to significant depositional hiatuses and differences in sedimentary facies, an age-depth one-to-one model was deemed unsuitable for the application. Rather a chronological framework was constructed by dividing the section into four depositional phases by combining the results of multi-climate proxies.

4.2 Grain size and multi-climate proxies result

Grain sizes within the aeolian deposition are likely influenced by multiple independent materialization processes (Újvári et al., 2016). Here, sand is defined as particle sizes >63 μm, while the particle sizes of clay do not exceed 2 μm. Sand fraction content fluctuates between 6.01% and 16.5% throughout the whole section. At depths of 390–140 cm, the fluctuation in sand fraction is intense, as evidenced by a variance of 5.12. It also has demonstrated a similar shifting trend as the mean grain size (MGZ) at the same depths (Figure 2). There are five distinct peaks with a rapid decrease followed by a slow increase in the sand fraction between two adjacent peaks. At this stage, changes in the clay fraction content were not significant. At depths of 140–90 cm, both the sand fraction content and MGZ showed a rapidly decreasing trend with a corresponding increase in the content of the clay component. At depths of 90–0 cm, the continuous decrease in MGZ shows an inverse trend relative to the change in clay fraction content. However, the sand fraction content is relatively stable (a variance of 3.28) and even increased slightly compared to the previous period. The above phenomenon suggests that the dominant factor controlling the grain size composition of the JRT section shifted at a cut-off of approximately 90 cm and played a

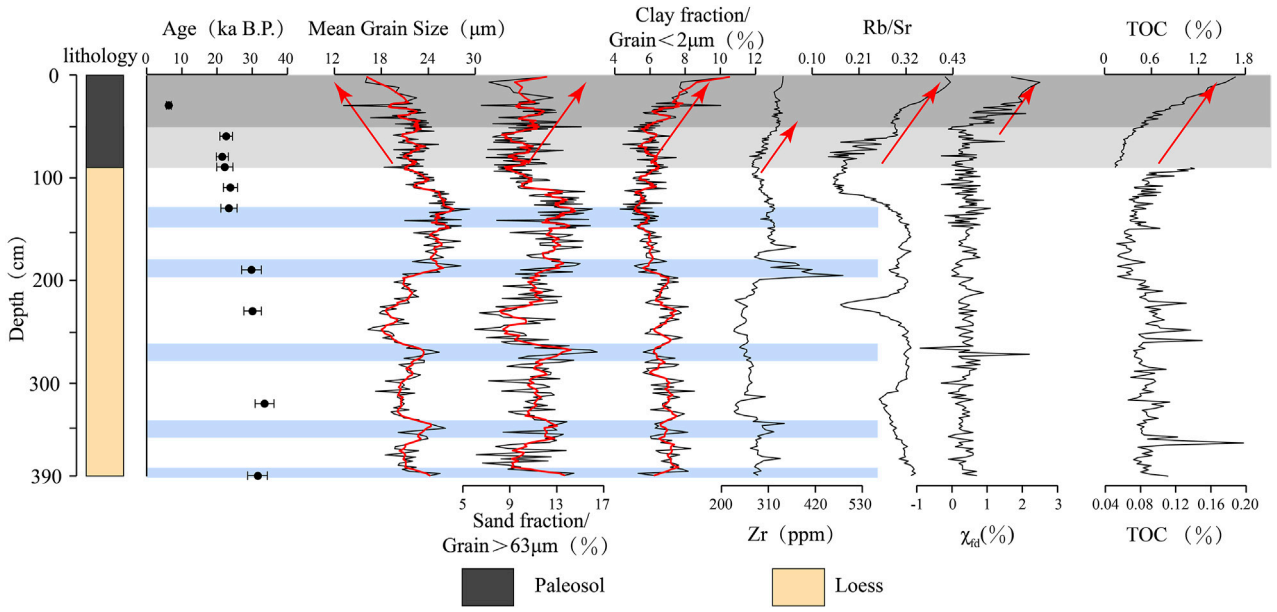

FIGURE 2
Grain size and multi-climate proxies result of the JRT section. The loess-paleosol sequence is determined by a combination of field observation and climate proxies; The two gray boxes indicate the sediments with soil-forming action and vegetation development; the red arrow marks the trend of each indicator in the paleosol; the red line is the smoothed curve obtained by the adjacency averaging method; the blue box contains the five high relatively high values of MGZ and sand fraction.

more important role above 50 cm (Figure 2). Their influence in the sediment size fraction characteristics of JRT section is that the coarse fraction contributes more to the MGZ in the depth of 390–90 cm, while the fine fraction dominates the MGZ in the 90–0 cm.

Because of their different chemical properties, the Rubidium/Strontium ratio (Rb/Sr) is always used to indicate the degree of chemical weathering (Gallet et al., 1996; Chen et al., 2001). Zirconium (Zr) is extremely stable during chemical weathering. Therefore, it is often used to indicate changes in sediment sources (Taylor and McLennan, 1985; Li et al., 2020). In the top ~50 cm of the JRT section, the content of Zr is stable, and the Rb/Sr is significantly higher than for sediments below 50 cm and is continuously increasing. This suggests that the formation of the upper sediment was accompanied by strong weathering and soil formation processes (Figure 2).

Soil TOC is closely related to input, burial time, and decomposition level (Meyers, 1997; Chen et al., 2005; Zhang and Liu, 2008). The parameter χ_{fd} responds to the content of superparamagnetic particles. Thereby indirectly reflecting the environmental characteristics and vegetative conditions (Liu et al., 1990). The significant change in TOC occurred at a depth of about 90 cm and followed by a rapid increase above that layer. Its corresponding change in χ_{fd} occurred at a depth of 50 cm. There phenomenon suggests the soil in the lower and central parts of JRT section is typical loess and not conducive to vegetation development. A top 50/90 cm paleosol layer developed in a warmer and wetter context and was accompanied by a significantly improved vegetation condition (Figure 2).

4.3 Chronological framework

Based on grain size and multi climate proxies results, we have divided the JRT section into four stages: Stage 1 at a depth (Sun and Wu, 1987) of 390–140 cm, stage 2 at 140–90cm, stage 3 at 90–50 cm, and stage 4 at 50 cm. Combined with OSL dating results, they belong to the Late MIS3, Early LGM, Late LGM, and Post Glacial, respectively (Figure 3).

4.4 Pollen data

We had identified 35 terrestrial pollen taxa from the JRT section. Arboreal pollen is dominated by *Pinus* and *Picea*, while *Artemisia* and Orthomorphic commonly account for more than 80% of non-arboreal pollen. Owing to the rarity of some pollen taxa, we have clearly marked only 14 species in the pollen diagrams (Figure 3).

Since less than 300 pollen grains can be identified in sediments below 90 cm. The following detailed description

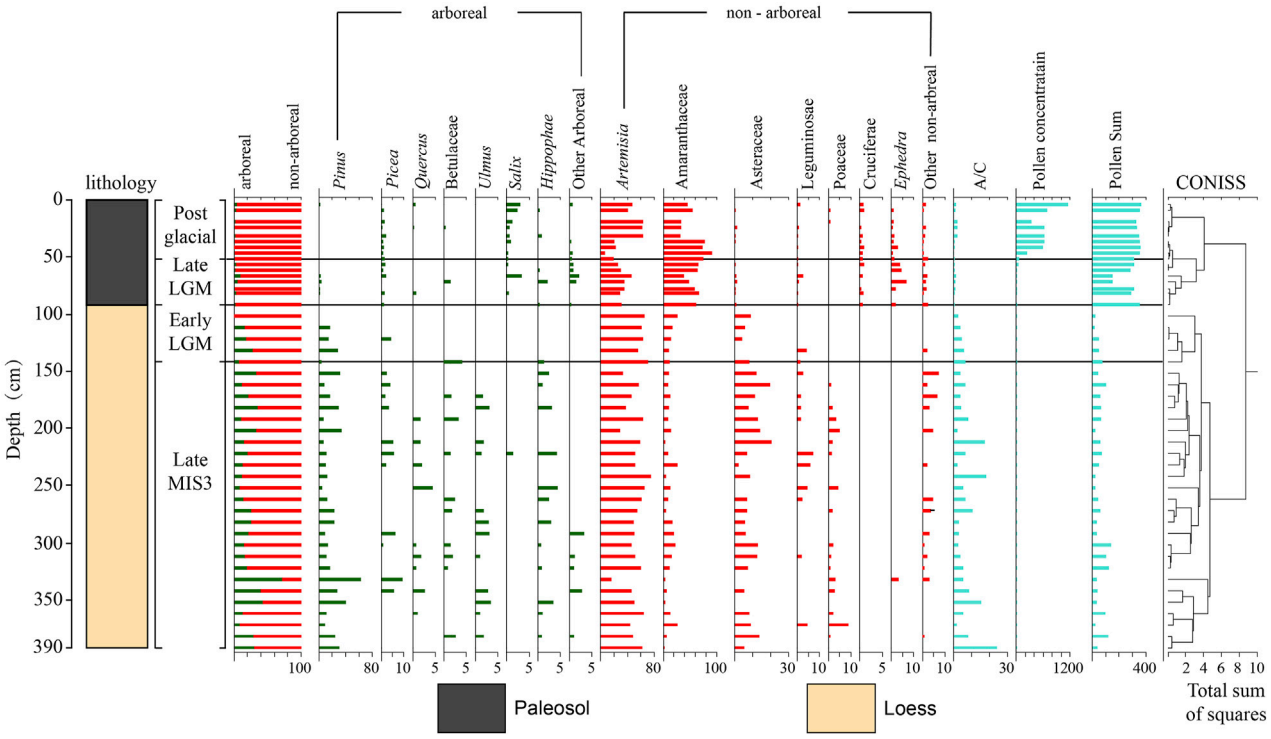

FIGURE 3
Percentage pollen diagram of selected taxa of JRT section. The four stages divided by the black line are based on OSL, grain size, and the results of multi-climate proxies, as described in Section 4.3.

and discussion of pollen are mainly based on the chronological framework established in Section 4.3. Pollen records from all strata within a stage are assumed to reflect the overall vegetation condition. We only compare the differences between the different stages to compensate for the lack of pollen number in individual strata.

4.4.1 Stage 1 (390–140 cm, late marine isotope stage 3)

At this stage, an average of 60.192 pollen per sample were identified. The pollen concentration is extremely low and the average concentration is only 7.722 grains/g. But there are relatively rich types of pollen. *Pinus*, *Artemisia*, and Asteraceae are the dominant pollen components. At the same time, pollen of *Picea*, *Quercus* and Betulaceae occasionally occurs in the sediment. In addition, the A/C (*Artemisia*/Chenopodiaceae) at this stage (7.528) is the highest in the entire record (Figure 3).

4.4.2 Stage 2 (140–90 cm, early last glacial maximum)

At this stage, an average of 34.5 pollen per sample were identified. The most important feature of this stage is an extremely monotonous pollen species. The dominant pollen component is *Artemisia* (55.102–70.270%). Amaranthaceae pollen tended to increase, while the percentage of *Pinus* pollen rapidly decrease (Figure 3).

4.4.3 Stage 3 (90–50 cm, late last glacial maximum)

Pollen of *Picea* and *Pinus* occurs simultaneously at this stage. The dominant component of pollen shifts to *Amaranthaceae* (56.898%). Cruciferae and *Ephedra* establish themselves as important components of non-arboreal pollen. Most notable is the significant overall increase in pollen concentration compared to the previous two stages (Figure 3).

4.4.4 Stage 4 (50–0 cm, Post glacial)

From 517.084 to 11447.727 grains/g, pollen concentration increased rapidly. Another notable change is that *Picea* has completely replaced *Pinus* as the most important arboreal pollen, but at a relatively low percentage (0.303–1.286%). *Artemisia* and Amaranthaceae are still the dominant pollen component. The sum of the percentages of these two pollen types is as high as 94.484%. In addition, *Ephedra* and *Salix* pollen are repeatedly present. The A/C shows an overall increasing trend, but the average value is only 0.947 (Figure 3).

5 Discussion

5.1 Pollen sources in the loess-paleosol sequence of the jirentai section

Judging and distinguishing the material source and sedimentary facies is one of the bases for applying fossil pollen characteristics to reconstruct vegetation history (Xu et al., 2015; Chevaliera et al., 2020). Factors such as the properties of the sediment and its geographical location influence the pollen source it receives (Luo et al., 2009; Huang et al., 2010; Zhang et al., 2022; Zhao et al., 2022). Based on field observation and multi-climate proxy results, we point out that the sediment in the JRT section can be distinguished in at least two distinct phases: A deep aeolian loess and a thin paleosol layer. The boundary between these two layers is at a depth of approximately 50 cm, and 90–50 cm represents the transition phase (Figure 3).

In the JRT section, the pollen assemblage of the loess layer is significantly different from that of in the paleosol. *Pinus*, *Artemisia*, Asteraceae and an abundance of other pollen species (e.g., *Picea*, Betulaceae, Poaceae) occur in the loess layer. *Artemisia* and *Amaranthaceae* are the absolute dominant components of fossil pollen in the paleosol layer. *Ephedra* and *Sliax* pollen attain higher proportions. In overall terms, species are more abundant but pollen concentration is lower in the loess layer in the JRT section, while the opposite is true in the paleosol (Figure 3).

Studies of pollen assemblages in modern surface soil and their relationships to vegetation carried out in the Ili Valley and surrounding areas have shown that *Pinus*, *Picea*, *Ephedra*, *Artemisia,* and Orthomorphic are reported to be over-represented. These types of pollen have high pollen production or can be spread over longer distances by wind (Yang et al., 2004; Luo et al., 2009; Zhao and Li, 2013; Niu et al., 2022). Therefore, the ecological significance of these pollen needs to be considered to the nature of the sediments and their geographical location.

As described in Section 3.1, the JRT section is a typical aeolian deposition close to the Kashi River's modern channel. The main transporting force for pollen sources of the JRT section were either wind-powered or hydrodynamic. Furthermore, changes in the local hydrological environment may also have led to vegetation conditions at micro-landscapes that exhibit different characteristics from those of the surrounding area.

In terms of aeolian dust dynamics alone, the rate of accumulation of Ili loess over the past 36 ka has been influenced mainly by the intensity of the Siberian High-pressure system. A strong Siberian high-pressure will drive cold air over the ACA and lead to frequent and intense dust activities in winter and spring (Ye et al., 2000; Orlovsky et al., 2005; Li et al., 2019; Kang et al., 2022; Li et al., 2022). In addition, the typical aeolian deposits of the Ili Valley are extremely poor for forming soil with poor vegetation cover (Li et al., 2020; Yang et al., 2020). During the Last Glacical, local and poorly developed vegetation provided only a very limited amount of pollen for the JRT section. Frequent dust activity facilitated pollen dispersal over longer distances (Figure 4C,F,G). *Pinus* is the most typical representative. Modern it do not grow in the Ili Valley and surrounding mountains. In the JRT section, a relatively high sand fraction content, the percentage of *Pinus* pollen, pollen concentration, and low A/C and TOC occur simultaneously at depths of 390–140 cm (Figure 4A–E). Therefore, we suggest the existence of a spatially extensive pollen source of fossil pollen within the loess layer of the JRT section and that the pollen assemblages exhibit regional vegetation characteristics.

During the Late LGM and Post Glacial, relatively high rates of soil deposition occurred in the middle to late Holocene in the Ili Valley (Kang et al., 2022). Because of weaker dust activity, this phenomenon is most likely attributed to an increase in effective moisture and the development of vegetation, thus enhancing the ability of the ground to trap dust (Figure 4G,H) (Chen et al., 2016; Cheng et al., 2017; Gao et al., 2019; Kang et al., 2020; Wang et al., 2020). The results of multi-climate proxies from the JRT section show a strong soil-forming tendency in the paleosol layer and a significantly higher TOC, which also responds to the development of local vegetation (Figure 2). Correspondingly, *Pinus* pollen in the paleosol layer has largely disappeared. The A/C ratio follows a similar trend to TOC and pollen concentration, with an overall increase (Figure 4A,B,D). Based on these evidences, we suggest that vegetation surrounding the JRT section was the main pollen source for the paleosol.

Based on the above discussion and the modern distribution of vegetation in the Ili Valley, we point out that frequent dust activities bring abundant pollen to the JRT section during the loess layer. *Picea* and *Pinus* are typical representatives. They grow in modern only in high altitude mountainous areas and far from the JRT section, but have high percentage of pollen in the loess layer. *Artemisia* is also the dominant pollen type at this stage and has been shown to be super-representative due to its high productivity and the ability to be dispersed over long distances (Xu et al., 2013; Xu and Zhang., 2013). However, a targeted study suggest that *Artemisia's* wind-dependent dispersal ability is much weaker than that of *Picea* and *Pinus*, and its over-representation can be attributed to its high productivity (Wang and Wang., 1983; Cai et al., 2014). The proportion of *Artemisia* and Amaranthaceae is stable in this phase and the A/C corresponds well to TOC. We hypothesize that it comes from a relatively small area. During the Late LGM and Post Glacial, the high percentage of pollen from Artemisia, Amaranthaceae and Ephedra, which may be dependent on the development of paleosols and grow near the JRT section. *Sailx* perhaps depends on wet areas in the Ili Valley such as along the Kash River. The almost disappearance of *Pinus* and the very low percentage of Picea reflect to the presence of spruce forests in mountainous areas.

Based on the above discussion, we also suggest that A/C can reflect the vegetation condition of the lowlands of the Ili Valley, although it differs in source areas at different stages.

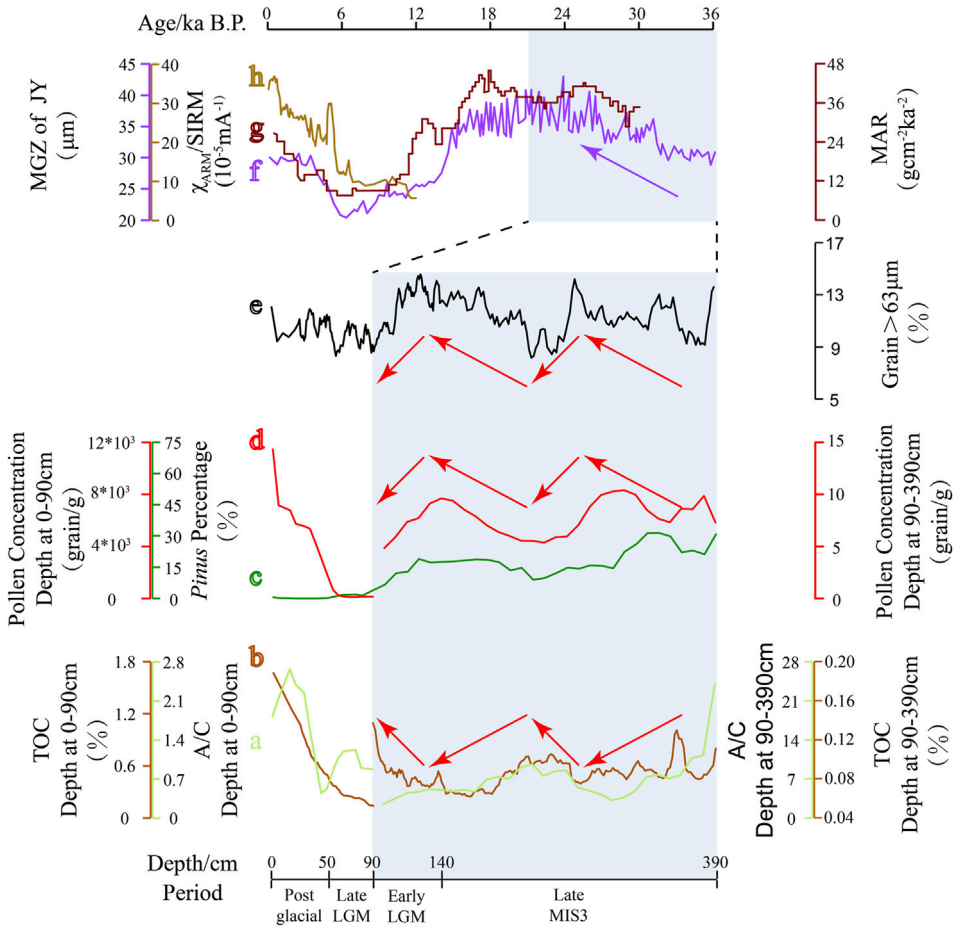

FIGURE 4
Comparison records of pollen assemblages, dust activity, and climate between JRT and ACA during the last 36 ka. **(A–E):** The smoothed curve obtained by the adjacency averaging method of TOC, A/C, pollen concentration (Bounded by a depth of 90 cm, these three proxies have significantly different values in the sediment. Thus, they were separated in the graph and set separately on the y-axis), the percentage of *Pinus* and sand fraction content of the JRT (this study). **(F):** Mean grain sizes of the Jingyuan loess section located in the northwestern China Loess Plateau (Sun et al., 2010); **(G)**: stacked mass accumulation rate (MAR) record in the Ili valley (Kang et al., 2022); **(H)**: the χ_{ARM}/SIRM ratio of the LJW10 Holocene paleosol section (Chen et al., 2016); The red arrows mark the trend of the climate proxies in the JRT section; The purple arrow marks the enhancing trend of Siberian High-pressure from Late MIS3 to LGM; The two blue bars represent the same time period, which is defined by the intensity of the stronger Siberian High-pressure.

5.2 Vegetation history in the Ili Valley during the last 36 ka

The pollen record from the JRT section provides a clear and brief history of vegetation in the eastern Ili Valley during the last 36 ka. We continue to base our analysis on the four stages described above and discuss its change process (Figure 3).

During the Late MIS3, the relatively stable and high percentage (mean of 51.296%) of *Artemisia* reflect the general desert-steppe status within the lowland areas of the Ili Valley. Moisture-loving *Asteraceae, Poaceae* and some arboreal plants (e.g., *Quercus, Betulaceae,* and *Ulmus*) may grow in localized areas with humid condition. The highest percentage of *Pinus* that occurs in this stage and has a very large variation (4.3%–62.5%), suggesting that *Pinus* forests were present in the surrounding mountains of the Ili Valley. Based on its relationship with TOC and sand fraction, we further suggest that the forest line may have declined when the environment deteriorated. The situation regarding *Picea* is similar to it. So stronger dust activities can carry more abundant pollen into the lowland areas.

Compared with the previous stage, the change of pollen concentration in the Early LGM is not obvious. However, the sustained increase in the percentage of *Amaranthaceae* suggests the deterioration of vegetation. The extremely monotonous pollen spectra (*Artemisia*, *Pinus*, *Asteraceae*) assemblage further confirms the phenomenon. The entirety of the lowland areas of the Ili Valley is dominated by typical desert vegetation. Sand fraction is still high in JRT section. Changes in

Pinus concentrations responded to the trend of diminishing dust activity, and *Picea* almost disappeared. These results may foreshadow the degradation of forests in the mountains.

The increase in pollen concentration reveals the initial development of vegetation surrounding the JRT section in the Late LGM. Amaranthaceae is the dominant local vegetation species. In addition, the typical drought-tolerant vegetation *Ephedra* occurred in the pollen spectra. This observation, when combined with the disappearance of Asteraceae and Poaceae, allows us to infer that the vegetation was a typical desert type at the early stage of soil formation surrounding the JRT section. Despite the further weakening of dust activity, the frequent occurrence of *Picea* pollen in the JRT section indicates the expansion of montane forests at this stage.

Changes in fossil pollen assemblage and concentration suggest that the vegetation condition surrounding the JRT section has improved remarkably during the Post Glacial. However, the worst vegetation condition surrounding the JRT section persisted into the Holocene, which differs markedly from the situation of the mountain forests. Counter-trending the changes in the content of *Artemisia* and *Amaranthaceae*, the percentage of *Ephedra* decrease slightly but is still present. *Salix* may grow along the Kashi River or be supported by groundwater, but it only represents the vegetation status of a micro-landscape. Among arboreal plants, only *Picea* and *Salix* play important roles. Although the weak dust activity is a cause, the average concentration of *Picea* pollen of less than 1% indicates that the *Picea* forests are far from the JRT section (Luo et al., 2009; Zhao and Li, 2013). In summary, the vegetation condition near the JRT section has improved significantly. It provides a large source of pollen for the JRT section. But it is a typical desert steppe or riverine meadow vegetation type.

5.3 Relationship between vegetation and climate change in the arid Central Asia during the last glacial maximum

An abundant and detailed vegetation history in the modern Interglacial can be obtained from the various sediments of the ACA. Along with the increased effective moisture during the middle and late Holocene, these records show some commonalities, such as a rich variety of pollen species, a reduction in the percentage of *Ephedra*, and an increase in both pollen concentration and the percentage of *Artemisia* pollen (Tarasov et al., 1997; Chen et al., 2008; Huang et al., 2009; Ran et al., 2015; Zhang and Feng, 2018; Wang and Zhang, 2019; Chen et al., 2019; Zhao et al., 2022).

However, with the decrease in solar radiation at high latitudes and the southward shift and weakening of westerly belt during the LGM (Berger and Loutre, 1991; Clark et al., 2009; Lei et al., 2021), precipitation and river runoff significantly decreased in the ACA. These factors limit the development of ideal fossil pollen carrier sediments such as lake and peat (Yang and Liu., 2003; Li et al., 2016; Zhang et al., 2016; Duan et al., 2018; Zhao et al., 2021). Studies from different regions have shown that small lake basins with short shorelines receive more endemic pollen than larger lake basins, and the mixing effect on pollen is weaker, which may lead to a poorer response of lake pollen assemblages to regional vegetation and climate change (Davis and Brubaker, 1973; Jacobson and Bradshaw, 1987; Sun and Wu, 1987; Jackson, 1990; Tian et al., 2009). Significant increases in sediment sand fraction indicate Lakes Ailike, Ebi, Manas, and Balikun have shrunk rapidly since the LGM. This phase generally lasted for nearly 10,000 years or even longer (Rhodes et al., 1996; Zhao et al., 2015; Jia et al., 2020; Chen and Liu., 2022). Some similar changes are also observed in the pollen records, such as the monotony of pollen types and the decrease in the proportion of *Pinus* and *Picea* (Figure 5). The above phenomena point to the vegetation near the lake basin become the main fossil pollen source because of the shrinking of the lake. This could also be attributed to the degradation of regional woodland vegetation features experienced during this time or a combination thereof. However, more detailed information can not be obtained from these lakes.

Our results effectively complement the vegetation history and its links to the climate of this period. Compared to the Late MIS3, significant vegetation degradation occurred in both the montane forest and the lowland desert steppe during the Early LGM. In the Late LGM, paleosols gradually developed around the JRT section. The presence of *Picea* in the pollen spectra also indicates the recovery of montane vegetation (Figure 4). These changes occurred significantly earlier than in the lake sediment records, but coincided with the increased insolation in the mid-to-high-latitude Northern Hemisphere (Berger and Loutre, 1991). Modern observations show that vegetation development at high latitudes in the Northern Hemisphere responds to increases in temperature and CO_2 concentration (Lucht et al., 2002; Piao et al., 2006). Therefore, we speculate that increased insolation in the Northern Hemisphere was a direct factor in the development of the montane forest zone in the ACA during the Late LGM. The corresponding increase in precipitation from glacial meltwater and westerly rapids has also effectively improved the vegetation conditions in the lowland areas of ACA.

However, the present information from the lake records indicates that the vegetation condition in the ACA began to degrade in the Early LGM. The phenomenon lasted for nearly 10,000 years or even longer (Figure 5). The process of global lake response to climate change in recent decades explains this phenomenon (Woolway et al., 2020). When the climate turns warm, the increased evaporation and the mean of precipitation or river recharge will exert a combined influence on the lake area. Higher evaporation rates will cause a decrease in lake level and reduction in surface water extent. Several of the lakes mentioned above are dependent on runoff and meltwater recharge. The changing conditions of these lakes of rapid warming in the Late LGM

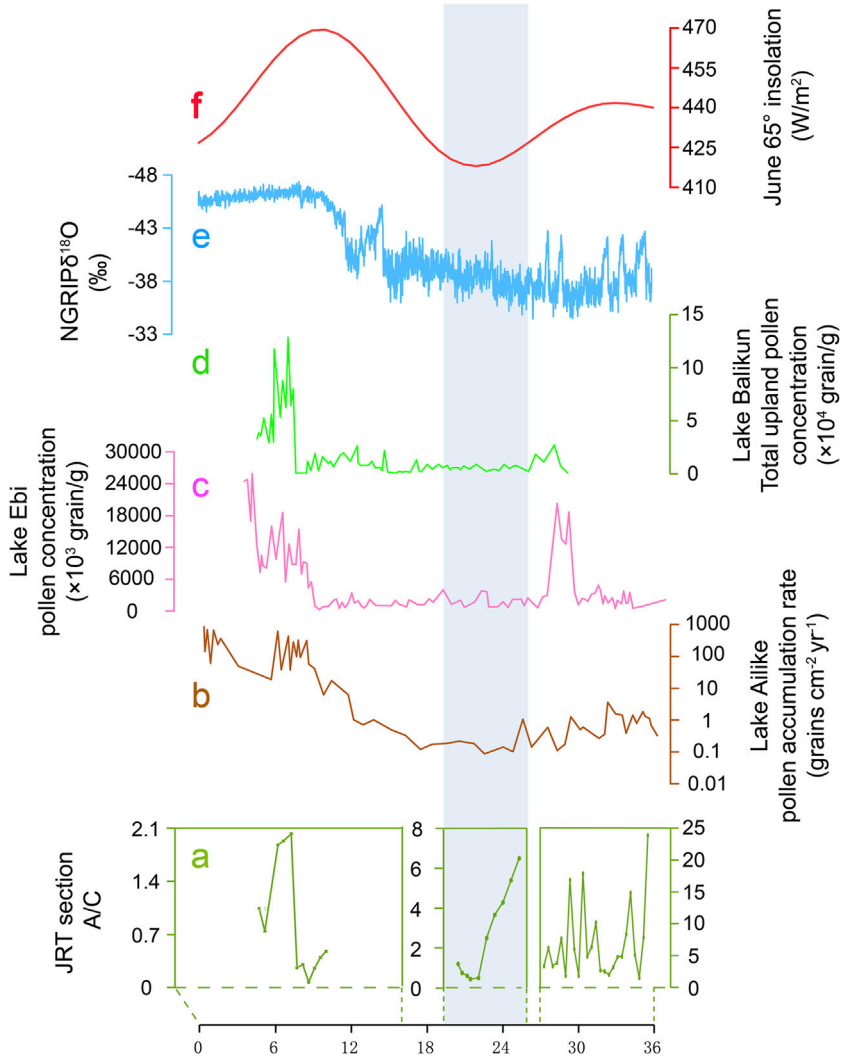

FIGURE 5
Comparison of the vegetation condition obtained from sediment fossil pollen reconstruction with climate records in the ACA. **(A)** A/C of the JRT section; **(B)** Pollen accumulation rate of Lake Ailike (Chen and Liu, 2022); **(C)** Pollen concentration of Lake Ebi (Jia et al., 2020); **(D)** Total upload pollen concentration of Lake Balikun (Tao et al., 2010; Zhao et al., 2015); **(E)** Greenland NGRIP $\delta^{18}O$ record on GICC053 1.0063 chronology (WAIS Divide Project Members, 2015); **(F)** Solar insolation at 65°N for July (Berger and Loutre, 1991). The blue bar represents the time of the LGM (Clark et al., 2009); The X-axis of the data from the JRT section uses a dashed line, which only represents that the corresponding data exists in an approximate time period.

and Post Glacial can be inferred from the patterns of change in lake states under global warming. More recharge and higher evaporation work together to affect the water balance of the lake, and a smaller lake area may have lasted longer and lagged behind the temperature rise during the Late LGM and Post Glacial (Figure 5). Endemic pollen is always the main pollen source in such lakes. When the regional vegetation was restored, the pollen record in these lakes could not respond effectively to this change.

To simplify, we designed a model diagram to express the differences in pollen response to vegetation and climate in loess-paleosol sequences and lake sediments in the ACA. Both the vegetation surrounding the depositional area and the region provide pollen sources for sediments mainly through the action of wind or water. Pollen assemblages from lakes during the interglacial and from the loess during the glacial are more likely to come from an enlarged area and tending to reflect the relationship between the regional vegetation and climatic conditions. When the climate changes, at least for a shift from cold-dry to warm-wet, the response of the lake state and its pollen assemblage is a lag (Figure 6).

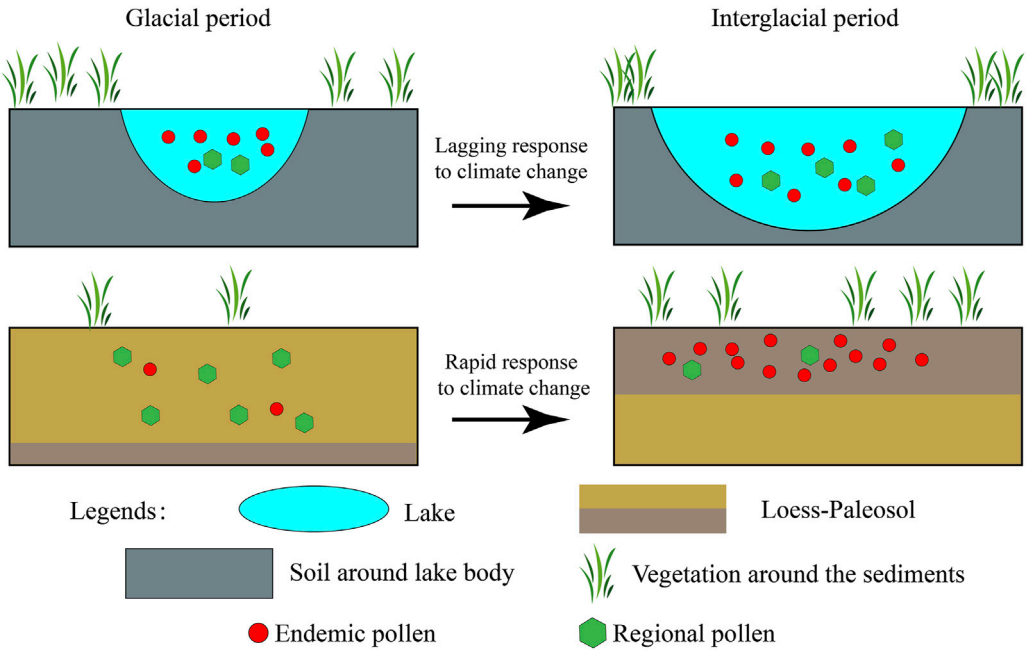

FIGURE 6
A model for expressing variation in pollen assemblages and responses to climate change in the lake and loess-paleosol sequence under ideal conditions.

6 Conclusions

A local/regional vegetation history was revealed by a loess-paleosol sequence in the eastern Ili Valley since the Late MIS3. In brief, the environment of lowland areas is always drought and harsh. Typical desert/desert steppe is dependent on rivers and groundwater. Mountainous forests can develop in suitable environments, such as the Late MIS3 and Post Glacial. In the Early LGM, significant vegetation deterioration occurred in both the lowland area of the valley and the mountains. Our results further show that vegetation restoration and environmental improvement occurred in the Late LGM and were attributed to increased Northern Hemisphere high-latitude insolation. This point in time is much earlier than previously known from lake sediments. A simple model diagram was designed to explain this phenomenon. We suggest that change in the loess-paleosol sequence and its pollen assemblage is more sensitive to vegetation and climate change during the transition from the glacial to interglacial.

Data availability statement

The raw data supporting the conclusions of this article will be made available by the authors, without undue reservation.

Author contributions

YM and ZL designed the study. MQ, QR, JL participated in the fieldwork. PL conducted the experiment and data analysis. PL, YM, ZL, SZ, and MQ wrote and revised the manuscript. All authors contributed to the article and approved the submitted version.

Funding

This research is supported by the Pan-Third Pole Environment Study for a Green Silk Road (Pan-TPE) (XDA2004010101), and the National Natural Science Foundation of China (NSFC, Grants No. 42030505, 42161144012).

Conflict of interest

The authors declare that the research was conducted in the absence of any commercial or financial relationships that could be construed as a potential conflict of interest.

Publisher's note

References

An, C. B., Tao, S. C., Zhao, J. J., Chen, F. H., Lv, Y. B., Dong, W. M., et al. (2013). Late Quaternary (30.7-9.0 cal ka BP) vegetation history in Central Asia inferred from pollen records of Lake Balikun, northwest China. *J. Paleolimnol.* 49 (2), 145–154. doi:10.1007/s10933-012-9649-7

Berger, A., and Loutre, M. F. (1991). Insolation values for the climate of the last 10 million years. *Quat. Sci. Rev.* 10 (4), 297–317. doi:10.1016/0277-3791(91)90033-Q

Cai, P., Wan, T., Han, X. L., Ge, Y. H., and Xu, Z. P. (2014). Research on pollen of Artemisia frigida spread. *Grassl. Prataculture* 26 (04), 26–29. doi:10.3969/j.issn.2095-5952.2014.04.007

Chen, F. H., Chen, J. H., Wang, W., Chen, S. Q., Huang, X. Z., Jin, L. Y., et al. (2019). Westerlies Asia and monsoonal Asia: Spatiotemporal differences in climate change and possible mechanisms on decadal to sub-orbital timescales. *Earth. Sci. Rev.* 192, 337–354. doi:10.1016/j.earscirev.2019.03.005

Chen, F. H., Huang, W., Jin, L. Y., Chen, J. H., and Wang, J. S. (2011). Spatiotemporal precipitation variations in the arid Central Asia in the context of global warming. *Sci. China Earth Sci.* 41 (11), 1812–1821. doi:10.1007/s11430-011-4333-8

Chen, F. H., J, J., Chen, J. H., Li, G. Q., Zhang, X. J., Xie, H. C., et al. (2016). A persistent Holocene wetting trend in arid central Asia, with wettest conditions in the late Holocene, revealed by multi-proxy analyses of loess-paleosol sequences in Xinjiang, China. *Quat. Sci. Rev.* 146, 134–146. doi:10.1016/j.quascirev.2016.06.002

Chen, F. H., Yu, Z. C., Yang, M. L., Ito, E., Wang, S. M., Madsan, D. B., et al. (2008). Holocene moisture evolution in arid central Asia and its out-of-phaserelationship with Asian monsoon history. *Quat. Sci. Rev.* 27 (3-4), 351–364. doi:10.1016/j.quascirev.2007.10.017

Chen, J., Wang, Y. J., Chen, Y., Liu, L. W., Ji, J. F., and Lu, H. Y. (2001). Rb and Sr geochemical characterization of the Chinese loess and its implications for palaeomonsoon climate. *Acta Geol. Sin.* 75 (02), 259–266. doi:10.1111/j.1755-6724.2000-02-025

Chen, Q. Q., Shen, C. D., Sun, Y. M., Peng, S. L., Yi, W. X., Li, Z. A., et al. (2005). Meahanism of distribution of soil organic matter with deoth due to evolution of soil profiles at the dinghushan biosphere reserve. *Acta. Pedol. Sin.* 42 (1), 1–8.

Chen, Y. R., and Liu, X. Q. (2022). Vegetation and climate changes since the middle MIS 3 inferred from a Lake Ailike pollen record, xinjiang, arid central Asia. *Quat. Sci. Rev.* 290, 107636. doi:10.1016/j.quascirev.2022.107636

Cheng, L. Q., Song, Y. G., Sun, H. Y., and Orzbaev, R. (2017). Spatio-temporal distribution of dust sedimentation rate of Tianshan loess since MIS3 and its implications. *Mar. Geol. Quat. Geol.* 39 (1), 143–153. doi:10.16562/j.cnki.0256-1492.2017032001

Chevaliera, M., Davisa, B. A. S., Heirib, O., Seppäc, H., Chase, B. M., Gajewski, K., et al. (2020). Pollen-based climate reconstruction techniques for late Quaternary studies. *Earth. Sci. Rev.* 210, 103384. doi:10.1016/j.earscirev.2020.103384

Clark, P. U., Dyke, A. S., Shakun, J. D., Carlson, A. E., Clark, J., Wohlfarth, B., et al. (2009). The last glacial Maximum. *Science* 325 (5941), 710–714. doi:10.1126/science.1172873

Davis, B. M., and Bruaker, L. B. (1973). Differential stedimentation of pollen grains in lakes. *Limnol. Oceanogr.* 18 (4), 635–646. doi:10.4319/lo.1973.18.4.0635

Ding, Z. L., Ranov, V., Yang, S. L., Finaev, J. M., Han, J. M., and Wang, G. A. (2002). The loess record in southern Tajikistan and correlation with Chinese loess. *Earth Planet. Sci. Lett.* 200 (3-4), 387–400. doi:10.1016/S0012-821X(02)00637-4

Duan, F. T., An, C. B., Zhao, Y. T., Zhang, X. N., Zhou, A. F., and Huang, X. Z. (2018). A preliminaey study on the climate change since the last interglaciation based on lake sediments from Xinjiang, Northwest China. *Quat. Sci.* 35 (5), 1156–1165. doi:10.11928/j.issn.1001-7410.2018.05.10

Fang, X. M., Shi, Z. T., Yan, M. D., Li, J. J., and Jiang, P. A. (2002). Loess in the tian Shan and its implications for the develop-ment of the Gurbantunggut Desert and drying of northern xinjiang. *Chin. Sci. Bull.* 47 (16), 1381–1387. doi:10.1360/02tb9305

Fordham, D. A., Jackson, S. T., Brown, S. C., Huntley, B., Brook, B. W., Dahl-Jensen, D., et al. (2020). Using paleo-archives to safeguard biodiversity under climate change. *Science* 363 (1072), eabc5654. doi:10.1126/science.abc5654

Gallet, S., John, B. M., and Toril, M. (1996). Geochemical characterization of the Luochuan loess-paleosol sequence, China, and paleoclimatic implications. *Chem. Geol.* 133 (1-4), 67–88. doi:10.1016/S0009-2541(96)00070-8

Gao, F. Y., Jia, J., Xia, D. S., and Wang, Y. J. (2019). Assessment of the dominant climatic factor affecting pedogenic development in eolian sequences during the Holocene in arid central Asia. *Quat. Int.* 502, 78–84. doi:10.1016/j.quaint.2018.04.039

Grimm, E. C. (1987). CONISS: A FORTRAN 77 program for stratigraphically constrained cluster analysis by the method of incremental sum of squares. *Comput. Geosci.* 13 (1), 13–35. doi:10.1016/0098-3004(87)90022-7

Grimm, E. C. (2004). *TILIA and TILIA.GRAPH v.2.0.2*. USA: Illinois State Museum, Spring-field.

Hu, Q., and Han, Z. H. (2022). Northward expansion of desert climate in central Asia in recent decades. *Geophys. Res. Lett.* 49 (11). doi:10.1029/2022GL098895

Huang, X. Z., Chen, F. H., Fan, Y. X., and Yang, M. L. (2009). Dry late-glacial and early Holocene climate in arid central Asia indicated by lithological and palynological evidence from Bosten Lake, China. *Quat. Int.* 194, 19–27. doi:10.1016/j.quaint.2007.10.002

Huang, X. Z., Zhou, G., Ma, Y. L., Xu, Q. H., and Chen, F. H. (2010). Pollen distribution in large freshwater lake of arid region: A case study on the surface sediments from Bosten lake, xinjiang, China. *Front. Earth Sci. China* 4 (2), 174–180. doi:10.1007/s11707-009-0060-2

Jackson, S. T. (1990). Pollen sourcearea and representation in small lakes of the Northeastern United States. *Rev. Palaeobot. Palynol.* 63, 53–76. doi:10.1016/0034-6667(90)90006-5

Jacobson, G. L., and Bradshaw, R. H. W. (1987). The selection of sites for paleovegetational studies. *Quat. Res.* 16 (1), 80–96. doi:10.1016/0033-5894(81)90129-0

Jia, H., Wu, J. L., Zhang, H., and Yi, S. (2020). Pollen-based climate reconstruction from Ebi Lake in northwestern China, Central Asia, over the past 37, 000 years. *Quat. Int.* 544, 96–103. doi:10.1016/j.quaint.2020.02.033

Kang, S. G., Wang, X. L., Roberts, H. M., Duller, G. A. T., Song, Y. G., Liu, W. G., et al. (2020). Increasing effective moisture during the Holocene in the semiarid regions of the Yili basin, central asia: Evidence from loess sections. *Quat. Sci. Rev.* 246, 106553. doi:10.1016/j.quascirev.2020.106553

Kang, S. G., Wang, X. L., Wang, N., Song, Y. G., Liu, W. G., Wang, D., et al. (2022). Siberian High modulated suborbitalscale dust accumulation changes over the past 30 ka in the eastern Yili Basin, Central Asia. *Paleoceanogr. Paleoclimatol.* 37, e2021PA004360. doi:10.1029/2021PA004360

Lai, Z. P., and Ou, X. J. (2003). Basic procedures of optically stimulated luminescence (OSL) dating. *Prog. Geogr.* 32, 683–693. doi:10.11820/dlkxjz.2013.05.001

Lei, J., Shi, Z. G., Xie, X. N., Shi, Y. Y., Li, X. Z., Liu, X. D., et al. (2021). Seasonal variation of the westerly Jet over asia in the last glacial Maximum: Role of the Tibetan plateau heating. *J. Clim.* 37 (7), 2723–2740. doi:10.1175/JCLI-D-20-0438.1

Li, C., Cao, Z. Z., Ding, L., Shi, Y., and Yang, Z. H. (2012). Climate change Characters in recent 50 Years in Yili valley xinjiang. *J. Shanxi Agric. Sci.* 40 (5), 508–514. doi:10.3969/j.issn.1002-2481.2012.05.23

Li, G. Q., Rao, Z. G., Duan, Y. W., Xia, D. S., Wang, L. B., Madsen, D. B., et al. (2016). Paleoenvironmental changes recorded in a luminescence dated loess/paleosol sequence from the Tianshan Mountains, arid central Asia, since the Penultimate Glaciation. *Earth Planet. Sci. Lett.* 448, 1–12. doi:10.1016/j.epsl.2016.05.008

Li, J. F. (1991). *Climate in Xinjiang*. Beijing: China Meteorological Press.

Li, L. Q., Kürschner, K. M., Lu, N., Chen, H. Y., An, P. C., and Wang, Y. D. (2022). Palynological record of the Carnian Pluvial Episode from the northwestern Sichuan basin, SW China. *Rev. Palaeobot. Palynol.* 304, 104704. doi:10.1016/j.revpalbo.2022.104704

Li, X. Q., Zhao, K. L., Dodson, J., and Zhou, X. Y. (2011). Moisture dynamics in central asia for the last 15 kyr: New evidence from Yili valley, xinjiang, NW China. *Quat. Sci. Rev.* 30 (23-24), 3457–3466. doi:10.1016/j.quascirev.2011.09.010

Li, Y., Piao, S. L., Li, L. Z. X., Chen, A. P., Wang, X. H., Ciais, P., et al. (2018). Divergent hydrological response to large-scale afforestation and vegetation greening in China. *Sci. Adv.* 4 (5), eaar4182. doi:10.1126/sciadv.aar4182

Li, Y., Song, Y. G., Fitzsimmons, K. E., Chen, X. L., Prud'homme, C., and Zong, X. L. (2020). Origin of loess deposits in the north tian Shan piedmont, central asia. *Palaeogeogr. Palaeoclimatol. Palaeoecol.* 559, 109972. doi:10.1016/j.palaeo.2020.109972

Li, Y., Song, Y. G., Kaskaoutis, D. G., Zhang, X. X., Chen, X. L., Shukurov, N., et al. (2022). Atmospheric dust dynamics over central asia: A perspective view from loess deposits. *Gondwana Res.* 109, 150–165. doi:10.1016/j.gr.2022.04.019

Li, Y., Song, Y. G., Qiang, M. R., Miao, Y. F., and Zeng, M. X. (2019). Atmospheric dust variations in the Ili basin, northwest China, during the last glacial period as revealed by a high mountain loess-paleosol sequence. *J. Geophys. Res. Atmos.* 124 (15), 8449–8466. doi:10.1029/2019JD030470

Liu, L. Y., and Zhang, X. (2021). *Global land-cover product with fine classification system at 30 M using time-Series Landsat Imagery V1.0*. Aerospace Information Research Institute, Chinese Academy of Sciences. doi:10.12237/casearth.6123651428a58f70c2a51e49

Liu, X. M., Liu, D. S., Heller, F., and Xu, T. C. (1990). Frequency-dependent susceptibility of loess and quaternary paleoclimate. *Quatern. Sci.* 10 (01), 42–50. doi:10.1007/s00376-999-0032-1

Lu, H. X., Liu, W. G., Yang, H., Wang, H. Y., Liu, Z. H., Leng, Q., et al. (2019). 800-kyr land temperature variations modulated by vegetation changes on Chinese Loess Plateau. *Nat. Commun.* 10, 1958. doi:10.1038/s41467-019-09978-1

Lucht, W., Prentice, I. C., Myneni, R. B., Stich, S., Friedlingsten, p., Cramer, W., et al. (2002). Climatic Control of the high-latitude vegetation greening trend and Pinatubo effect. *Science* 296 (5573), 1687–1689. doi:10.1126/science.1071828

Luo, C. X., Zheng, Z., Tarasov, P., Pan, A. D., Huang, K. Y., Beaudouin, C., et al. (2009). Characteristics of the modern pollen distribution and their relationship to vegetation in the Xinjiang region, northwestern China. *Rev. Palaeobot. Palynol.* 153, 282–295. doi:10.1016/j.revpalbo.2008.08.007

Marx, S. K., Kamber, B. S., Mcgowan, H. A., Petherick, L. M., Mctainsh, G. H., Stromsoe, N., et al. (2018). Palaeo-dust records: A window to understanding past environments. *Glob. Planet. Change* 165, 13–43. doi:10.1016/j.gloplacha.2018.03.001

Meyers, P. A. (1997). Organic geochemical proxies of paleoceanographic, paleolimnologic, and paleoclimatic processes. *Org. Geochem.* 27 (5-6), 213–250. doi:10.1016/S0146-6380(97)00049-1

Miao, Y. F., Warny, S., Clift, P. D., Liu, C., and Gregory, M. (2017). Evidence of continuous Asian summer monsoon weakening as a response to global cooling over the last 8 Ma. *Gondwana Res.* 52, 48–58. doi:10.1016/j.gr.2017.09.003

Mottl, O., Flantua, S., Bhatta, K. P., Felde, V. A., Giesecke, T., Goring, S., et al. (2021). Global acceleration in rates of vegetation change over the past 18, 000 years. *Science* 372 (6544), 860–864. doi:10.1126/science.abg1685

Murray, A. S., and Wintle, A. G. (2000). Luminescence dating of quartz using an improved single-aliquot regenerative-dose protocol. *Radiat. Meas.* 32 (1), 57–73. doi:10.1016/S1350-4487(99)00253-X

Narisma, G. T., Foley, J. A., Licker, R., and Ramankutty, N. (2007). Abrupt changes in rainfall during the twentieth century. *Geophys. Res. Lett.* 34, 067100–L7316. doi:10.1029/2006GL028628

Niu, D. Y., Li, J. Y., Wang, N. L., Du, J. F., and Chen, X. J. (2022). Relationship between pollen assemblages in surface soil and modern vegetation and climate in the Western Tianshan Mountains, Xinjiang. *J. Glaciol. Geocryol.* 44 (3), 1–13. doi:10.7522/j.issn.1000-0240.2022.0088

Orlovsky, L., Orlovsky, N., and Durdyev, A. (2005). Dust storms in Turkmenistan. *J. Arid. Environ.* 60, 83–97. doi:10.1016/j.jaridenv.2004.02.008

Piao, S. L., Friedlingstein, P., Ciais, P., Zhou, L. M., and Chen, A. P. (2006). Effect of climate and CO2 changes on the greening of the Northern Hemisphere over the past two decades. *Geophys. Res. Lett.* 33, L23402. doi:10.1029/2006GL028205

Prospero, J. M., Ginoux, P., Torres, O., Nicholson, S. E., and Gill, T. M. (2002). Environmental characterization of global sources of atmospheric soil dust identified with the NIMBUS 7 Total Ozone Mapping Spectrometer (TOMS) absorbing aerosol product. *Rev. Geophys.* 40 (1), 1–31. doi:10.1029/2000rg000095

Ran, M., Zhang, C. J., and Feng, Z. D. (2015). Climatic and hydrological variations during the past 8000 years in northern Xinjiang of China and the associated mechanisms. *Quat. Int.* 358, 21–34. doi:10.1016/j.quaint.2014.07.056

Rhodes, T. E., Gasse, F., Lin, R. F., Fonts, J. C., Wei, K. Q., Bertrand, P., et al. (1996). A late Pleistocene-Holocene lacustrine record from lake Manas, Zunggar (northern xinjiang, Western China). *Palaeogeogr. Palaeoclimatol. Palaeoecol.* 120, 105–121. doi:10.1016/0031-0182(95)00037-2

Shi, Y. F., Shen, Y. P., Kang, E., Li, D. L., Ding, Y. J., Zhang, G. W., et al. (2007). Recent and future climate change in northwest China. *Clim. Change* 80, 379–393. doi:10.1007/s10584-006-9121-7

Siegfried, T., Bernauer, T., Guiennet, R., Sellars, S., Robertson, A. W., Mankin, J., et al. (2012). Will climate Change exacerbate or mitigate water stress in central Asia? *Clim. Change* 112, 881–899. doi:10.1007/s10584-011-0253-z

Song, Y. G., Li, Y., Cheng, L. Q., Zong, X. L., Kang, S. G., Ghafarpour, A., et al. (2021). Spatio-temporal distribution of quaternary loess across central asia. *Palaeogeogr. Palaeoclimatol. Palaeoecol.* 567 (110279), 110279. doi:10.1016/j.palaeo.2021.110279

Sun, X. J., and Wu, Y. S. (1987). Distribution and quantity of sporopollen and algae in surface sediments of the Dianchi lake, Yunnan Preovince. *Mar. Geo. Quat. Geo.* 7 (04), 83–94.

Sun, Y. B., Wang, X. L., Liu, Q. S., and Clemens, S. C. (2010). Impacts of post-depositional processes on rapid monsoon signals recorded by the last glacial loess deposits of northern China. *Earth Planet. Sci. Lett.* 289 (1–2), 171–179. doi:10.1016/j.epsl.2009.10.038

Tang, L. Y., Mao, L. M., Shu, J. W., Li, C. H., Shen, C. M., and Zhou, Z. Z. (2016). *An Illustrated Handbook of Quaternary pollen and spores in China*. Beijing: Science Press.

Tao, S. C., An, C. B., Chen, F. H., Tang, L. Y., Wang, Z. L., Lü, Y. B., et al. (2010). Pollen-inferred vegetation and environmental changes since 16.7 ka BP at Balikun Lake, Xinjiang. *Chin. Sci. Bull.* 55 (22), 2449–2457. doi:10.1007/s11434-010-3174-8

Tarasov, P. E., Jolly, D., and Kaplan, J. O. (1997). A continuous Late Glacial and Holocene record of vegetation changes in Kazakhstan. *Palaeogeogr. Palaeoclimatol. Palaeoecol.* 136, 281–292. doi:10.1016/S0031-0182(97)00072-2

Taylor, S. R., and McLennan, S. M. (1985). *The continental crust: Its composition and Evolution*. Oxford: Blackwell.

Tian, F., Xu, Q. H., Li, Y. C., Cao, X. Y., Wang, X. L., and Zhang, L. Y. (2009). Pollen assemblage characteristics of lakes in the monsoon fringe area of China. *Sci. Bull. (Beijing).* 54 (4), 3354–3363. doi:10.1007/s11434-008-0408-0

Tian, Z. P., Zhuang, L., and Li, J. G. (2012). The vertical distribution of vegetation patterns and its relationship with environment factors at the northern slope of Ili river valley: A bimodal distribution pattern. *Acta eco. Sin.* 32 (4), 1151–1162. doi:10.5846/stxb201012271856

Újvári, G., Kok, J. F., Varga, G., and Kovács, J. (2016). The physics of wind-blown loess: Implications for grain size proxy interpretations in Quaternary paleoclimate studies. *Earth. Sci. Rev.* 154, 247–278. doi:10.1016/j.earscirev.2016.01.006

Uno, I., Eguchi, K., Yumimoto, K. E., Takemura, T., Shimizu, A., Uematsu, M., et al. (2009). Asian dust transported one full circuit around the globe. *Nat. Geosci.* 2 (8), 557–560. doi:10.1038/ngeo583

WAIS Divide Project Members (2015). Precise interpolar phasing of abrupt climate change during the last ice age. *Nature* 520, 661–665. doi:10.1038/nature14401

Wang, F. X., Qian, N. F., Zhang, Y. L., and Yang, H. Q. (1995). *Pollen Flora of China*. Beijing: Science Press.

Wang, K. F., and Wang, X. Z. (1983). *Introduction to sporology*. Beijing: Peking University Press.

Wang, Q., Wei, H. T., Khormali, F., Wang, L. B., Yan, H. Y., Xie, H. C., et al. (2020). Holocene moisture variations in Western arid central Asia inferred from loess records from NE Iran. *Geochem. Geophys. Geosyst.* 21 (3). doi:10.1029/2019GC008616

Wang, W., and Feng, Z. D. (2013). Holocene moisture evolution across the Mongolian plateau and its surrounding areas: A synthesis of climatic records. *Earth. Sci. Rev.* 122, 38–57. doi:10.1016/j.earscirev.2013.03.005

Wang, W., and Zhang, D. L. (2019). Holocene vegetation evolution and climatic dynamics inferred from an ombrotrophic peat sequence in the southern Altai Mountains within China. *Glob. Planet. Change* 179, 10–22. doi:10.1016/j.gloplacha.2019.05.003

Woolway, R. I., Kraemer, B. M., Merchant, C. J., O'Reilly, C. M., and Sharma, S. (2020). Global lake responses to climate change. *Nat. Rev. Earth Environ.* 1, 388–403. doi:10.1038/s43017-020-0067-5

Wu, L. P., Yang, Y. H., Yang, J. Y., Feng, X. C., and Zeng, K. K. (2018). Analysis of precipitation variation characteristics in Kashi River basin in Ili Valley. *J. AnHui Agric. Sci.* 50 (10), 190–194. doi:10.3969/j.issn.0517-6611.2022.10.043

Xia, H. F., Xie, H. B., Liu, H., Wen, G. C., and Li, W. (2018). Relations of vegetation with topography and groundwater in Yili river valley of xinjiang. *J. Yangtze River Sci. Res. Inst.* 35 (9), 54–57. doi:10.11988/ckyyb.20170133

Xinjiang Expedition Team Chinese Academy of Sciences (1978). *Vegetation and its Utilization in Xinjiang*. Beijing: Sciences Press.

Xu, Q. H., Cao, X. Y., Tian, F., Zhang, S. R., Li, Y. C., Li, M. Y., et al. (2013). Relative pollen productivities of typical steppe species in northern China and their potential in past vegetation reconstruction. *Sci. China Earth Sci.* 43 (12), 1254–1266. doi:10.1007/s11430-013-4738-7

Xu, Q. H., Li, M. Y., Zhang, S. R., Zhang, Y. H., Zhang, P. P., and Lu, J. Y. (2015). Modern pollen processes of China: Progress and problems. *Sci. Sin. -Terrae.* 45 (11), 1661–1682. doi:10.1360/zd2015-45-11-1661

Xu, Q. H., and Zhang, S. R. (2013). A clear advance in Soft Actuators Advances in Earth Science. *Science* 28 (9), 968–969. doi:10.1126/science.1243314

Xu, Y. J., Chen, Y. N., Li, W. H., Fu, A. L., Mao, X. D., and Gui, D. W. (2010). Distribution pattern and environmental interpretation of plant species diversity in the mountainous region of Ili River Valley, Xinjiang, China. *Chin. J. Plant Ecol.* 34 (10), 1142–1154. doi:10.3773/j.issn.1005-264x.2010.10.003

Yang, H., Li, G. Q., Huang, X., Wang, X. Y., Zhang, Y. N., Jonell, T. N., et al. (2020). Loess depositional dynamics and paleoclimatic changes in the Yili Basin, Central Asia, over the past 250 ka. *Catena* 195, 104881. doi:10.1016/j.catena.2020.104881

Yang, X. P., and Liu, D. S. (2003). Palaeoenvironments in desert regions of northwest China around 30 ka B.P. *Quat. Sci.* 23 (1), 6. doi:10.3321/j.issn:1001-7410.2003.01.003

Yang, Z. J., Kong, Z. C., Yan, S., Ni, J., Ma, K. P., and Xu, Q. H. (2004). Pollen distribution in Topsoil along the Daxigou Valley in the Headwaters of the Urumqi river the central Tianshan mountains. *Arid. Land Geogr.* 27 (4), 543–547. doi:10.3321/j.issn:1000-6060.2004.04.017

Yao, T. D., Thom, L. G., Shi, Y. F., Qin, D. H., Jiao, K. Q., Yang, Z. H., et al. (1997). A study of climate change records since the last interglacial in the Guria ice core[J]. *Sci. Sin. (Terrae)* (05), 447–452.

Ye, W., Dong, G. R., Yuan, Y. J., and Ma, Y. J. (2000). Climate instability in the Yili region, Xinjiang during the last glaciation. *Chin. Sci. Bull.* 45 (6), 1604–1609. doi:10.1007/bf02886222

Ye, W. (2001). *The characteristics and Paleaoclimate of loess deposits in westerly are*. Beijing: Ocean Press.

Youn, J. H., Seong, Y. B., Choi, J. H., Abdrakhmatov, K., and Ormukov, C. (2014). Loess deposits in the northern Kyrgyz tien Shan: Implications for the paleoclimate reconstruction during the late quaternary. *Catena* 117, 81–93. doi:10.1016/j.catena.2013.09.007

Zhang, D. L., and Feng, Z. D. (2018). Holocene climate variations in the Altai mountains and the surrounding areas: A synthesis of pollen records. *Earth. Sci. Rev.* 185, 847–869. doi:10.1016/j.earscirev.2018.08.007

Zhang, L., Yang, Lin., Zohner, C. M., Crowther, T. W., Li, M. C., Shen, F. X., et al. (2022). Direct and indirect impacts of urbanization on vegetation growth across the world's cities. *Sci. Adv.* 8, eabo0095. doi:10.1126/sciadv.abo0095

Zhang, P., and Liu, W. G. (2008). Loess sedimentary organic matter records from the central chines loess plateau and the implication of C/N ratio. *Mar. Geol. Quat. Geol.* 28 (06), 119–124. doi:10.3724/SP.J.1140.2008.06119

Zhang, S. R., Sun, Y. H., Li, M. Y., Wang, N., and Xu, Q. H. (2022). Paleovegetation and paleotemperature in North China during the mid-Holocene based on sedimentological and palynological evidence from Lake Baiyangdian. *Palaeogeogr. Palaeoclimatol. Palaeoecol.* 595, 110982. doi:10.1016/j.palaeo.2022.110982

Zhang, X. N., Zhou, A. F., Zhang, C., Hao, S. T., Zhao, Y. T., and An, C. B. (2016). High-resolution records of climate change in arideastern central Asia during MIS 3 (51 600-25 300 cal a BP) from Wulungu Lake, north-Western China. *J. Quat. Sci.* 31 (6), 577–586. doi:10.1002/jqs.2881

Zhang, Y. P., Zhang, J. F., Ruan, Q. R., Wang, Y. Q., Han, J. Y., Zhang, J. N., et al. (2021). Geomorphological background and formation process of the Goukou site in Jirentai, Xinjiang[J]. *Quateanary. Sci.* 41 (5), 1376–1393. doi:10.11928/j.issn.1001-7410.2021.05.13

Zhao, K. L., Li, X. Q., Dodson, J., Zhou, X. Y., and Atahan, P. (2013). Climate instability during the last deglaciation in central Asia, reconstructed by pollen data from Yili Valley, NW China. *Rev. Palaeobot. Palynol.* 189, 8–17. doi:10.1016/j.revpalbo.2012.10.005

Zhao, K. L., and Li, X. Q. (2013). Modern pollen and vegetation relationships in the Yili basin, xinjiang, NW China. *Chin. Sci. Bull.* 58, 4133–4142. doi:10.1007/s11434-013-5896-x

Zhao, K. L., Li, X. Q., Xu, H., Zhou, X. Y., Dodson, J., and Liu, J. C. (2019). Increased winter-spring precipitation from the last glaciation to the Holocene inferred from a δ13Corg record from Yili Basin (Xinjiang, NW China). *Sci. China Earth Sci.* 62, 1125–1137. doi:10.1007/s11430-018-9333-x

Zhao, Y. T., An, C. B., Mao, L. M., Zhao, J. J., Tang, L. Y., Zhou, A. F., et al. (2015). Vegetation and climate history in arid Western China during MIS2: New insights from pollen and grain-size data of the Balikun Lake, eastern Tien Shan. *Quat. Sci. Rev.* 126, 112–125. doi:10.1016/j.quascirev.2015.08.027

Zhao, Y. T., An, C. B., Zhou, A. F., Zhang, X. N., Zhao, J. J., Dong, W. M., et al. (2021). Late Pleistocene hydroclimatic variabilities in arid north-west China: Geochemical evidence from Balikun lake, eastern Tienshan, China. *J. Quat. Sci.* 36 (3), 415–425. doi:10.1002/jqs.3288

Zhao, Y. T., Miao, Y. F., Lei, Y., Cao, X. Y., and Xiang, M. X. (2021). Progress, problems and prospects of palynology in reconstructing environmental change in inland arid areas of Asia. *Sci. Cold Arid Regions* 13 (4), 271–291. doi:10.3724/SP.J.1226.2021.20049

Zhao, Y. T., Miao, Y. F., Li, Y., Fang, Y. M., Zhao, J. J., Wang, X. L., et al. (2022). Non-linear response of mid-latitude Asian dryland vegetation to Holocene climate fluctuations. *Catena* 213 (106212), 106212. doi:10.1016/j.catena.2022.106212